NIH Public Access
Author Manuscript
Nat Neurosci. Author manuscript; available in PMC 2013 May 01.

Published in final edited form as:
Nat Neurosci. 2012 November ; 15(11): 1524–1530. doi:10.1038/nn.3235.

OLM interneurons differentially modulate CA3 and entorhinal inputs to hippocampal CA1 neurons

Richardson N Leão[1,2], **Sanja Mikulovic**[1], **Katarina E Leão**[1,2], **Hermany Munguba**[2], **Henrik Gezelius**[1], **Anders Enjin**[1], **Kalicharan Patra**[1], **Anders Eriksson**[1], **Leslie M. Loew**[3], **Adriano BL Tort**[2], and **Klas Kullander**[1,4]

[1]Developmental Genetics, Department of Neuroscience, Uppsala University, Box 593, 751 24 Uppsala, Sweden

[2]Brain Institute, Federal University of Rio Grande do Norte, Natal, RN 59056, Brazil

[3]R. D. Berlin Center for Cell Analysis and Modeling, UConn Health Center, Farmington, CT 06030, United States

[4]Science for Life Laboratory, Department of Neuroscience, Uppsala University, Box 593, 751 24 Uppsala, Sweden

Abstract

The vast diversity of GABAergic interneurons is believed to endow hippocampal microcircuits with the required flexibility for memory encoding and retrieval. However, dissection of the functional roles of defined interneuron types have been hampered by the lack of cell specific tools. Here we report a precise molecular marker for a population of hippocampal GABAergic interneurons known as oriens lacunosum-moleculare (OLM) cells. By combining novel transgenic mice and optogenetic tools, we demonstrate that OLM cells have a key role in gating the information flow in CA1, facilitating the transmission of intrahippocampal information (from CA3) while reducing the influence of extrahippocampal inputs (from the entorhinal cortex). We further demonstrate that OLM cells are interconnected by gap junctions, receive direct cholinergic inputs from subcortical afferents, and account for the effect of nicotine on synaptic plasticity of the Schaffer collateral pathway. Our results suggest that acetylcholine acting through OLM cells can control the mnemonic processes executed by the hippocampus.

Introduction

The hippocampus is a brain region involved in spatial navigation and memory formation[1,2], but the network mechanisms underlying these functions are not well understood. Recent evidence suggests that the control of pyramidal cell (PC) activity by GABAergic interneurons is critically required for the execution of hippocampal functions[3,4]. Hippocampal interneurons are a diverse population of cell types, which have distinct post-synaptic domains and thus differentially control input/output activity[5]; the precise roles played by the distinct inhibitory cell types are currently unclear. The classification of hippocampal interneurons through their expression of proteins and peptides including parvalbumin (PV), calretinin (CR), calbindin (CB), somatostatin (SOM), vasoactive

Correspondence and requests for materials should be addressed to Klas.Kullander@neuro.uu.se or Richardson.Leao@neuro.uu.se.

Author Contributions

HG, AEn and KK designed and produced the transgenic mice. RL, KL, AT, LL and KK designed the experiments. RL, KL, SM, HM, KP and AEr performed the experiments. RL, KL, AT and KK analyzed data and wrote the paper.

The authors declare that no competing financial interest exists.

NIH-PA Author Manuscript
NIH-PA Author Manuscript
NIH-PA Author Manuscript

NIH-PA Author Manuscript

NIH-PA Author Manuscript

NIH-PA Author Manuscript

intestinal peptide (VIP), and neuropeptide Y (NPY) has been a major framework for studying interneuron function[6,7]. However, to date no single molecular marker is specific for any interneuron subtype, as defined by their pattern of PC innervation. For example, PV+ cells include basket, bistratified and axo-axonic cells[6], which target PCs at different subcellular compartments. In light of modern genetic techniques that can enhance or suppress cellular activity[8], finding specific molecular markers for morphologically well-defined subtypes of GABAergic interneurons is extremely valuable for understanding their role in information processing.

Oriens lacunosum-moleculare (OLM) cells are a major class of GABAergic interneurons in the outermost layer of the hippocampus (stratum oriens - SO) with perpendicular axonal projections to the innermost layer (stratum lacunosum-moleculare - SLM)[5]. CA1 OLM cells inhibit the distal apical dendrites of PCs, the same cellular compartment where the direct input originating from layer III of the entorhinal cortex (EC) arrives, forming the temporoammonic (TA) pathway[9]. OLM cells have been hypothesized to coordinate cell assemblies[10] and to produce theta oscillations[11,12], cross-frequency coupling[10,13], and gating of long-term potentiation (LTP)[14]. However, despite insights derived from computer simulations[10,15], the function of OLM cells has not been directly demonstrated.

Importantly, OLM cells are highly sensitive to nicotine[14], but it is currently unknown whether cholinergic neurons from the medial septum and diagonal band of Broca (MS-DBB), the major source of acetylcholine to the hippocampus, directly target nicotine receptors in OLM cells. To our knowledge, no functional study has yet shown fast cholinergic inputs originating from the MS-DBB to any known type of hippocampal neuron. It is currently believed that subcortical cholinergic afferents are mainly neuromodulatory, acting through slow metabotropic receptors[16]. *In vitro*, however, nicotine facilitates LTP of Schaffer collateral (SC) synapses onto CA1 PCs through receptors containing the nicotinic acetylcholine receptor α2 subunit (CHRNA2) that are exclusively present in SO[14,17,18]. Recent evidence suggests that CHRNA2 may be specifically expressed in OLM cells, which in turn could underlie the enhancement of SC-CA1 LTP by nicotine[14,19]. Thus, direct cholinergic excitation of OLM cells might be involved in switching the information flow in the CA1 from direct EC inputs carrying sensory information (TA pathway) to inputs carrying internal representations stored in CA3 (SC pathway)[15].

To investigate this hypothesis, we generated a mouse line expressing Cre recombinase under the control of the *Chrna2* promoter (Chrna2-cre). Here we show that *Chrna2* is a molecular marker specific for CA1 OLM cells in the hippocampus. Further, we demonstrate that CA1 OLM cells inhibit distal portions of CA1 PC dendrites while disinhibiting proximal dendrites, modulate synaptic efficiency and plasticity of EC and CA3 inputs, and are excited by fast cholinergic transmission.

Results

OLM cells were observed already by Ramon y Cajal, but their network function remains elusive. To date, the most used marker for OLM cells is SOM; however, SOM is also expressed in other interneuron subtypes found in SO as well as in *stratum pyramidale* (SP) and *stratum radiatum* (SR) of CA1 and CA3, and in the dentate gyrus[5] (Supplementary Fig. 1). A recent study hypothesized that CHRNA2 may be specifically expressed in OLM cells[14]. Consistent with this, *in situ* hybridization has shown that *Chrna2* mRNA is restrictively found at CA1 SO in the hippocampus of mice[17]. To investigate whether *Chrna2* is a specific marker of CA1 OLM cells, we generated a mouse line expressing Cre recombinase under the control of the *Chrna2* promoter (Chrna2-cre). Histological analysis of the hippocampi of mice expressing the red fluorescent protein Tomato under the control of

NIH-PA Author Manuscript

NIH-PA Author Manuscript

NIH-PA Author Manuscript

Cre (Chrna2-cre/*R26*^{tom}) showed that Tomato+ cells in the hippocampus were almost exclusively located in the SO of CA1 and subiculum (Fig. 1a andSupplementary Fig. 1a), while cells positive for *somatostatin* mRNA (*som*) were found in multiple strata of all hippocampal regions (Supplementary Fig. 1b). *In situ* hybridization for *som* combined with immunohistochemistry for Tomato revealed that the vast majority (95.1%, 214/225 cells) of Tomato+ cells were also *som*+ and comprised a subpopulation (35.2%, 214/608) of CA1 *som*+ interneurons (Supplementary Fig. 1c and d).

Reconstructions of biocytin filled Tomato+ neurons (Fig. 1b) typically (87.6%, 148/169) displayed OLM cell morphology, i.e. cell bodies and horizontal dendrites in SO and axons running perpendicularly to SLM, where they branched considerably and terminated. The remaining neurons had morphologies compatible with pyramidal cells (4.1%), and trilaminar (4.1%), bistratified (1.8%) and SR (2.4%) interneurons. Tomato+ cells (n=126) displayed mean input resistance of 293.3±9.6MΩ, resting membrane potential of −60.3±0.3mV, capacitance of 31.5±0.7pF, low frequency discharge and a 'sag' in response to hyperpolarizing current injection (Fig. 1b), which are membrane properties typical of OLM cells[20]. These neurons fired spontaneous action potentials (APs) at low frequencies (1.1±0.2Hz in whole cell recordings, n=15; 4.3±1.0Hz in cell attached recordings, n=10). Single cell reverse transcriptase PCR to detect glutamic acid decarboxylase 67 mRNA (n=25/25) and *in situ* hybridization for vesicular inhibitory amino acid transporter (*Viaat*) mRNA (Supplementary Fig. 2a) confirmed the inhibitory nature of the Tomato+ cells. Together, these results demonstrate that Chrna2-cre driven Tomato+ expression is highly specific for OLM cells in the CA1 region and subiculum. These cells are hereafter referred to as OLM$^{\alpha 2}$ cells.

OLM cells gate CA1 inputs

Morphological and electrophysiological data have shown that OLM cells exert strong inhibition onto distal portions of PC apical dendrites[9]. To corroborate these findings, we loaded PCs with the intracellular voltage sensitive dye (VSD) JPW3028[21] and QX314 (to block APs) while triggering APs in connected OLM$^{\alpha 2}$ cells. Depolarization of dendrites was achieved by PC somatic current injection (100pA, 400ms). We examined the spatial distribution of OLM$^{\alpha 2}$ cell inhibition onto PC dendrites by triggering APs in connected OLM$^{\alpha 2}$ cells at the end of the PC depolarization current step. As expected, we found that OLM$^{\alpha 2}$ cell spikes inhibit PCs mainly at the distal apical dendrite (mean fluorescence change in the distal dendrite: 0.6±0.02%$\Delta F/F_0$ vs. 0.4±0.04%$\Delta F/F_0$, n=4, t_3=8.36, p=0.0036, paired t-test; no significant change in fluorescence was found in proximal PC dendrites; Supplementary Fig. 3). We next investigated whether basal OLM$^{\alpha 2}$ cell activity influences EC inputs. Here we used voltage imaging with an extracellular VSD (RH795) to measure the spread of excitation - defined as the fluorescence change ratio between SR and SLM - following TA pathway stimulation (Fig. 1c). We then compared the spread of excitation in Chrna2-cre mice with mice in which inhibition from OLM$^{\alpha 2}$ cells was removed (by crossing Chrna2-cre mice with mice carrying a *Viaat* floxed allele[22] - *Viaat*^{lx}; see Methods and Supplementary Fig. 2b). Chrna2-cre/*Viaat*^{lx} mice exhibited a 13.7 fold increase in voltage spread from SLM to SR upon TA stimulation (0.57±0.06 of SLM $\Delta F/F_0$ in Chrna2-cre/*Viaat*^{lx} mice vs 0.04±0.01 in Chrna2-cre mice; n=6, t_5=7.03, p<0.001, t-test; Fig. 1c). These data suggest that OLM$^{\alpha 2}$ cells control the efficacy of EC inputs by targeted inhibition of PC distal dendrites.

In addition to inhibiting SLM, a recent study proposed that OLM cells would have an opposite effect in SR by inhibiting interneurons that target PC at the same dendritic compartments as the SC synapses[14], thus disinhibiting CA3 inputs. We tested whether activation of OLM$^{\alpha 2}$ cells can increase the excitatory effect of SC inputs by optogenetically activating OLM$^{\alpha 2}$ cells while recording electrical activity in PC dendrites using an

NIH-PA Author Manuscript

NIH-PA Author Manuscript

NIH-PA Author Manuscript

extracellular VSD (DI-4-ANBDQPQ)[23]. Of note, this red-shifted VSD was designed to have excitation spectrum different from channelrhodopsin (ChR) activation[23]. ChR expression in OLM cells was achieved by transducing $OLM^{\alpha 2}$ cells of Chrna2-Cre mice with a Cre-activated ChR2 variant H134R (hChR2) using adeno-associated viral vectors[24]. Viral production of hChR2 was restricted to $OLM^{\alpha 2}$ cells expressing Cre by using the double flox/inverse hChR2 frame strategy, as well as anatomically restricting the injection of the virus to CA1 (Supplementary Fig. 4a–c). In addition, light pulses were limited to SO by using a beveled optical fiber positioned ~2mm above the slice surface. Current clamp recordings showed that 400ms blue (473nm) light pulses triggered APs in ChR2-expressing $OLM^{\alpha 2}$ (OLM^{ChR2}) cells at frequencies that were directly dependent on light intensity. For example, in current clamp recordings, 1.4mW of laser power (at the tip of the fiber) generated 0.7±0.5 APs/pulse while 4.7mW pulses triggered 8.2±1.0APs/pulse (Supplementary Fig. 4d and e). Longer 1.4mW laser pulses (5 min) produced a moderate firing rate adaptation in OLM^{ChR2} cells (cell attached recordings; mean AP frequency: 4.3±1.0Hz without light, 8.4±0.7Hz and 6.3±0.9Hz during the 1st and 5th minute following light onset, respectively; $p<0.001$ when comparing the 1st and 5th min, paired t-test, $t_9=5.03$, $n=10$, Supplementary Fig. 4f).

By using the red-shifted VSD, we found that light activation of OLM^{ChR2} cells strongly suppressed the response to TA pathway stimulation (Control: 8.7±1.4$\Delta F/F_0$.s, Light: 3.0±1.1$\Delta F/F_0$.s, $p=0.006$, paired t-test, $t_4=5.28$, $n=5$, Supplementary Fig. 5). On the other hand, stimulation of the SC pathway led to a stronger depolarization in SR when OLM^{ChR2} cells were firing (Control: 1.3±1.1$\Delta F/F_0$.s, Light: 4.5±0.4$\Delta F/F_0$.s, $p=0.05$, paired t-test, $t_4=2.69$, $n=5$, Fig. 1d), consistent with a disinhibitory role of OLM cells[14]. To confirm this, we patched apical dendrites of PC in SR while stimulating SC inputs, holding the membrane potential at −60 mV (close to the Cl^- reversal potential of our recording solution). Consistent with VSD data, dendritic voltage clamp recording (in the presence of dAP5 to avoid dendritic spikes) revealed that light activation of OLM^{ChR2} cells leads to larger excitatory postsynaptic currents (EPSCs) summation in dendrites of PCs in SR (measured as the area under the curve of AMPA EPSCs produced by 11 SC stimulation pulses at 20 Hz; Light off: 1.7±0.3 pA.s; Light on: 2.2±0.2 pA.s, p=0.02, paired t-test, $t_4=3.60$, n=5; Fig. 1e).

Previously, it has been shown that SC excitation leads to feedforward inhibition onto PCs[25,26]. SC-associated SR interneurons are strong candidates for providing feedforward inhibition to PCs[25]. We next tested whether $OLM^{\alpha 2}$ cells - SR interneuron connections exist. Light stimulation of OLM^{ChR2} cells elicited inhibitory postsynaptic currents (IPSCs) in 6 out of 6 SR interneurons (31.5±0.7pA), which could be blocked by PTX (Fig. 2a). The 'feedforward' classification of these SR interneurons was subsequently confirmed by (1) presence of monosynaptic excitatory postsynaptic potentials (EPSPs) induced by SC stimulation, and (2) inhibition of PC dendrites upon their activation. SC stimulation produced EPSPs of 7.5±0.3mV in SR interneurons, with a delay (pulse time to 10% EPSP amplitude) of 1.6±0.04ms ($n=6$ cells; Fig. 2b). To visualize the effect of SR interneuron synapses on PC dendrites, we developed an electroporation technique to fill PC dendrites with VSD. We found that pulses of SC stimulation induced phasic depolarizations of PC dendrites, which were significantly lowered by the spiking of a single SR interneuron (from 1.7±0.2$\Delta F/F_0$ to 1.2±0.2$\Delta F/F_0$, $p=0.01$, paired t-test, $t_5=3.84$, $n=6$; Fig. 2b). Reconstruction of these interneurons showed cell bodies near the border of SR and SLM, with axonal arborizations predominantly confined to SR (Fig 2c). In line with electrophysiological data (Fig. 2a), confocal images revealed close proximity between $OLM^{\alpha 2}$ cell axons and SR interneuron dendrites (Fig. 2c). In addition to SC-associated SR interneurons, we also found connections from OLM^{ChR2} cells to 7 out of 16 bistratified cells (i.e., interneurons with axons targeting PC dendrites in SR[27]; mean IPSC: 48.1±6.8pA; Fig. 2d). Therefore, $OLM^{\alpha 2}$

NIH-PA Author Manuscript

NIH-PA Author Manuscript

NIH-PA Author Manuscript

cells are likely to increase PC electrogenesis upon SC stimulation through disinhibition of proximal PC dendrites.

Together, our results demonstrate that OLM$^{\alpha 2}$ cells may differentially control synaptic efficacy of EC and CA3 inputs onto CA1: when active, OLM$^{\alpha 2}$ cells inhibit TA inputs while concomitantly favoring SC synapses.

OLM$^{\alpha 2}$ cells differently modulate LTP in SC and TA pathways

The dual role of OLM$^{\alpha 2}$ cells in proximal and distal PC dendritic compartments could differentially affect plasticity in the SC-CA1 and the TA-CA1 pathway. We next studied the effect of OLM α 2cells on synaptic potentiation induced by the weak theta burst stimulation (wTBS) protocol. We found that light activation of OLM^{ChR2} cells (1.4mW laser power) for a 5-min period prior to and during TA wTBS largely attenuated the induction of synaptic potentiation in the TA-CA1 pathway (p=0.04 at t=30 min after wTBS, t-test, t_6=2.59, n=4 per group; Fig. 3). We then performed this experiment in Chrna2-cre/*Viaat*^{lx} mice. Importantly, OLM^{ChR2} cells in Chrna2-cre/*Viaat*^{lx} mice showed no significant difference in firing properties and response to light in comparison to cells from Chrna2-cre mice (Supplementary Fig. 4a–e). We found that TA-CA1 potentiation was highly facilitated in Chrna2-cre/*Viaat*^{lx} mice transduced with hChR2 independently of light activation (p=0.01 at t=30 min after wTBS, t-test, t_6=3.39, n=4 per group; Fig. 3 andSupplementary Fig. 6). Thus, these results show that OLM α 2cell activation inhibits potentiation of the TA-CA1 pathway.

OLM cells could also modulate plasticity of SC inputs by the disinhibitory mechanism described above (see also ref. 14). This hypothesis was tested by applying wTBS in SC before and after light activation of OLM^{ChR2} cells. We found that light activation was necessary to facilitate LTP (p=0.004 at t=30 min, t-test, t_7=4.17, n=4–5 per group), while SC wTBS alone was insufficient to produce LTP (Fig. 4a). Light activation of OLM^{ChR2} cells in Chrna2-cre/*Viaat*^{lx} animals had no effect on SC-CA1 LTP (Fig. 4a andSupplementary Fig. 7a). Interestingly, wTBS of SC inputs elicits LTP if nicotine is present in the perfusate[14]. OLM cells are likely to mediate the facilitation of LTP induction by nicotine due to their particular sensitivity to nicotine[28]. Consistent with previous findings[14], wTBS in the presence of nicotine induced LTP in the SC-CA1 synapse (p=0.017 at t=30 min after wTBS, t-test, t_9=2.92, n=5–6 per group; Fig. 4b and Supplementary Fig. 7b). However, this effect was absent in Chrna2-cre/*Viaat*^{lx} mice (Fig. 4b andSupplementary Fig. 7b), demonstrating that VIAAT mediated inhibition from OLM$^{\alpha 2}$ cells is required for the effect of nicotine on LTP. Of note, current clamp recordings showed that OLM$^{\alpha 2}$ neurons respond similarly to SC stimulation during nicotine or light application (n=11, Supplementary Fig. 7c and d). In all, our results demonstrate that OLM$^{\alpha 2}$ cells strongly facilitate LTP in the SC-CA1 pathway and suppress LTP in the TA-CA1 pathway.

OLM$^{\alpha 2}$ cells receive direct cholinergic inputs

We next sought to determine potential network mechanisms that could indirectly modulate CA3 and EC inputs by controlling the activity of CA1 OLM cells. In agreement with previous findings[29], local PC depolarization produced EPSCs (recorded at −60mV) in OLM$^{\alpha 2}$ cells (mean amplitude: −109.3±8.7 pA; n=8/15 pairs). Additionally, spikes in bistratified or trilaminar interneurons in CA1 SO elicited IPSCs in OLM$^{\alpha 2}$ cells with an average magnitude of 67.6±7.8 pA (n=7/25 pairs). A previous study has shown that gap junctions exist among SOM+ cells[30]. Consistent with this, paired recordings of OLM$^{\alpha 2}$ cells in Chrna2-cre/*R26*^{tom} mice with applied presynaptic voltage steps ranging from −80mV to 0mV produced outward currents in the presynaptic cell and inward currents postsynaptically (n=4/21 pairs). The mean junctional conductance calculated by $g = -I_{Post}/(V_{Pre} - V_{Post})$[31]

NIH-PA Author Manuscript

NIH-PA Author Manuscript

NIH-PA Author Manuscript

was equal to 0.7±0.1nS (Supplementary Fig. 8) and the coupling coefficient was 0.13±0.03 (n=4; measured in the cell with the lowest R_M). These findings corroborate that OLM$^{\alpha 2}$ cells receive both local excitation and inhibition and are connected by gap junctions.

We next assessed extrahippocampal inputs to OLM$^{\alpha 2}$ cells by stimulating the TA and fimbria fornix (FF) pathways. TA stimulation did not produce synaptic activity in OLM$^{\alpha 2}$ cells (n=21). In contrast, FF stimulation generated synaptic currents in 5 out of 23 cells in CA1 (but not in the subiculum n=0/17) with average amplitude of −46.3±5.4 pA. EPSC decay time constants could be fit with a double exponential function (fast and slow time constants = 2.4±0.3 and 12.7±2.6ms). The EPSCs were resistant to the AMPA receptor (r) blocker CNQX, NMDAr blocker dAP5, and GABAr blocker PTX (Fig. 5a). Application of the CHRNA7 blocker MLA lowered the EPSC amplitude to −12.5±2.7 pA (p=0.01, paired t-test, t_4=4.24, n=5, Fig. 5a), while a subsequent application of the unspecific nicotinic receptor antagonist MEC blocked the remaining current. Paired pulse stimulation of the FF caused a moderate facilitation of EPSCs in OLM$^{\alpha 2}$ cells (paired pulse ratio of 1.19±0.05 for a 25ms inter-pulse interval and 0.98±0.04 for a 200ms interval, p=0.02, paired t-test, t_4=3.54, n=5, Fig. 5b). Fibers arising from the MS-DBB, traveling through the FF, terminate in CA1 SO[32]. However, the neurotransmitters involved and the cellular targets of these inputs have not previously been characterized. Our results show that EPSCs in OLM$^{\alpha 2}$ cells evoked by FF stimulation are mediated by ionotropic cholinergic receptors, with an important contribution from the α 7 subunit.

Taken together, we conclude that cholinergic projections from the MS-DBB can directly excite OLM cells. This effect is modulated by local excitation and inhibition, and is likely to be amplified by gap junctions.

Discussion

OLM cells constitute a large GABAergic interneuron population in the hippocampus, but their network function remains poorly understood. Here we showed that OLM cells in CA1 are characterized by the expression of Chrna2. A novel Chrna2-Cre mouse line allowed us to identify and control OLM cells. We provided functional evidence that OLM cells inhibit PC dendritic compartments localized at SLM, reducing the strength of the direct input from EC layer III. In addition, we demonstrated that OLM cells inhibit SR interneurons that synapse on proximal PC dendritic compartments, suggesting that OLM cells counteract SC feedforward inhibition. Moreover, we showed that OLM cells suppress LTP in the TA-CA1 pathway while facilitating LTP in the SC-CA1 pathway. Together, our findings suggest that OLM interneurons can control the information flow into CA1 PCs by modulating direct sensory inputs from EC and internal inputs originating from CA3 (Supplementary Fig. 9).

Chrna2 is, to our knowledge, the most specific marker of a morphologically well-defined hippocampal interneuron population to date. Other markers, such as PV, are shared by different classes of interneurons[5,33]; in particular, SOM, an often used marker for OLM cells, is also expressed by other interneuron types such as bistratified and hilar perforant path-associated cells[5,34]. Further, SOM is expressed by interneurons in all hippocampal subregions, while Chrna2 expression is restricted to CA1 and subiculum (Supplementary Fig. 1). Nevertheless, the generation of PV-cre and SOM-cre mouse lines[35] has been a major advance for the study of interneuron function in oscillatory activity and behavior[3,4,36,37]; more selective markers such as the one described here should allow the study of the specific cell types within the larger population of PV+ and SOM+ cells.

Using extra- and intracellular voltage dye imaging, we demonstrated that OLM cells inhibit distal PC dendrites at SLM, as expected from anatomical data (Fig. 1 and Supplementary

NIH-PA Author Manuscript

NIH-PA Author Manuscript

NIH-PA Author Manuscript

Fig. 1). Less trivial, voltage imaging of SR and dendritic patch clamp recordings have shown that OLM cells disinhibit proximal PC dendrites. This result suggested a connection between OLM cells and dendritic inhibiting CA1 interneurons. This connection was confirmed by optogenetic stimulation of OLM cells, which led to IPSCs in two types of dendritic inhibiting interneurons: bistratified cells in SO and SC-associated interneurons in SR near the border of SLM. These connections are likely to account for the enhanced depolarization produced by SC stimulation when OLM cells are active. In contrast, a recent study showed that the removal of inhibition arising from SOM+ neurons increases the amplitude of SC EPSPs[38]. However, since SOM is not a specific marker of OLM cells, this effect could derive from decreased inhibition from other interneuron subtypes, such as bistratified cells or other dendritic targeting interneurons that are supplied with SC inputs[39]. In addition, since the PC dendrite is notoriously active[40], EPSCs sourced at the proximal PC dendrite could generate dendritic spikes in SLM. In this scenario, decreased inhibition from SOM+ interneurons could increase the net effect of SC stimulation by increasing tonic excitation and the generation of dendritic spikes.

How might OLM cells be controlled? It has previously been shown that OLM cells receive local excitation[29] and inhibition[38]. We here demonstrated that stimulation of the FF can elicit cholinergic EPSCs in CA1 OLM$^{\alpha 2}$ cells. The FF carries fibers originating from the MS-DBB, the main subcortical source of acetylcholine to the hippocampus[41]; hence, these results suggest a direct connection between cholinergic neurons in the MS-DBB and OLM$^{\alpha 2}$ cells in CA1. We hypothesize that acetylcholine acting on OLM$^{\alpha 2}$ cells could gate the information flow in CA1 by favoring the decoding of information stored in CA3 via the SC-CA1 synapse, while suppressing sensory information from the TA pathway. It should be noted that OLM cells express other nicotinic receptor subunits apart from Chrna2, such as Chrna7, which seem more influential in mediating the cholinergic responses of OLM cells (Fig. 5a). While we here focused on the network properties of OLM cells, making use of Chrna2 as a marker, the function of Chrna2 in OLM cells should be explored in future studies.

It has been previously hypothesized that OLM cells mediate LTP facilitation by nicotine[14]. Here we showed that optogenetic activation of OLM$^{\alpha 2}$ cells facilitate SC-CA1 LTP after wTBS in a manner similar to nicotine application. Conversely, nicotine had no effect on LTP in animals where VIAAT mediated transmission was specifically removed from OLM$^{\alpha 2}$ cells (Fig. 4). These results suggest that OLM$^{\alpha 2}$ cells account for the effect of nicotine on synaptic plasticity and also suggest that OLM$^{\alpha 2}$ cells have a pivotal role in mediating the memory enhancing effects of nicotine observed *in vivo*[42]. LTP in the TA-CA1 pathway, on the other hand, was suppressed by optogenetic stimulation of OLM$^{\alpha 2}$ cells (Fig. 3), whereas the selective removal of GABAergic transmission from OLM$^{\alpha 2}$ cells enhanced LTP induction in this pathway (Fig. 3). It should be cautioned, however, that the hippocampal network of Chrna2-cre/*Viaat*^{lx} mice may harbor potential compensatory changes. In any event, the results indicate that OLM$^{\alpha 2}$ cells provide inhibitory control over direct EC inputs. Hence, a greater influence of EC inputs over CA1 PCs could be achieved by turning off the background activity of OLM cells. It is important to note that although OLM cells fire tonically around theta frequency in slices[11] (Supplementary Fig. 4f), it remains to be established whether OLM cells can also be tonically activated by neuromodulators *in vivo*.

The opposite effects of OLM$^{\alpha 2}$ cells on SC-CA1 and TA-CA1 plasticity is likely explained by a local modulation of intracellular Ca^{2+} levels in different PC dendritic compartments. Ca^{2+} is one of the main signals for the induction of LTP/LTD[43], and a direct inhibition of PCs at the distal dendrites would likely lower Ca^{2+}concentration by closing voltage-gated

NIH-PA Author Manuscript

NIH-PA Author Manuscript

NIH-PA Author Manuscript

Ca^{2+} channels, while a disinhibition of the proximal dendrites should help increasing Ca^{2+} levels by the opposite mechanism[43].

In summary, we have shown that hippocampal Chrna2 is specifically expressed in OLM cells of the CA1 region and subiculum, which allowed dissecting their role in regulating synaptic plasticity of the hippocampal microcircuitry. Given that OLM cell dysfunction has been linked to epilepsy[44], schizophrenia[45], and cognitive impairment[46], manipulations of hippocampal CHRNA2 can potentially be used as a target for novel therapeutic strategies.

Online Methods

Mice

Chrna2-cre transgenic C57BL6 mice were generated by introducing the *Cre* gene at the ATG site of the first coding exon (middle of exon2) of the *Chrna2* gene in a Bacterial Artificial Chromosome (BAC, RP23–48P22). The protocols used and information of the bacterial strain (EL250) are available on http://recombineering.ncifcrf.gov. A plasmid containing nls-Cre-SV40 polyA-FRT-Kan/Neo-FRT was generated as a PCR template (information on request). Successful introduction of the Cre construct into the BAC was confirmed with PCR using the primers GACAGCCATTTTCTCGCTTC and AGGCAAATTTTGGTGTACG in a standard PCR reaction, the same primers were subsequently used for genotyping of the mice. BAC plasmid length was analyzed by enzyme restriction (2 h, 37°C), followed by Pulse Field Gel Electrophoresis (PFGE, CHEF mapper, Bio-Rad) 6V/h, 18h, 120° switch, 1–20s switch time. Validation sequencing of the BAC construct was made with custom designed primers covering the modified region (MWG-Biotech AG, Ebersberg, Germany). The modified BAC was linearized by NotI and purified as described in Marshall et al[48]. Briefly, the BAC DNA was separated with PFGE followed by β-agarase (NEB) digestion and dialysis to exchange the buffer to injection buffer. The modified BAC, which includes ~100 kbp upstream and ~8 kbp downstream of the *Chrna2* gene as well as all introns, was linearized by cleaving with NotI and introduced randomly into the mouse genome by pronuclear injection at Uppsala University Transgenic Facility (UUTF), which resulted in a founder line with expression of Cre in cells expressing CHRNA2 protein. *Viaat*^{lx} mice[22] and *Gt(ROSA)26Sor*$^{tm14(CAG-tdTomato)Hze}$ (*R26*^{tom}; Allen Brain Institute) mice have been described elsewhere. All animal procedures were approved by the appropriate local Swedish ethical committee (Jordbruksverket). Efforts were made to minimize the numbers of animals used.

Electrophysiology

Transverse hippocampal slices were obtained from P21–P30 Chrna2-cre/*R26*^{tom} and wild type littermate mice, Chrna2-cre/*Viaat*^{lx} mice, and 1–2 month-old hChR2 carrying mice of either sex (see *Virus injection*) as previously described and according to the rules of Animal Experimentation of the Uppsala University. Slices were maintained in artificial CSF (in mmol: 124 NaCl, 3.5 KCl, 1.25 NaH_2PO_4, 1.5 $MgCl_2$, 1.5 $CaCl_2$, 24 $NaHCO_3$, 10 glucose), constantly bubbled with 95% O_2 and 5% CO_2. Borosilicate glass electrodes (resistance = 4–8MΩ for somatic recordings; 12–18MΩ for dendritic recordings) were filled with either K-gluconate or CsCl-based internal solution[49]. Current/voltage clamp recordings were obtained from using either a Dagan BVC700 (Dagan), Axopatch 200B or a Multiclamp 700B (Molecular Devices) amplifiers; data was acquired by National Instruments DAQ cards and winWCP (Dr John Dempster, Strathclyde University, UK). No differences between firing and passive membrane properties and morphology of CA1 OLM cells were found between Chrna2-cre and WT littermates (n=153 cells); therefore, data is presented only from mice carrying Cre recombinase. Postsynaptic currents were obtained in voltage

NIH-PA Author Manuscript

NIH-PA Author Manuscript

NIH-PA Author Manuscript

clamp at a holding potential of −60mV using a CsCl-based internal solution (Cl^- reversal potential = 0mV).

Extracellular field EPSP (fEPSP) recordings (LTP experiments) were obtained by placing a concentric stimulation electrode (FHC) either at SR or SLM (for SC or TA stimulation, respectively) as previously described[14]. A borosilicate glass pipette (4–8MΩ) filled with ACSF was used to record SC or TA fEPSPs at the CA1 region 200–400 μm away from the stimulation electrode. Stimulation strength was adjusted to obtain 50–60% of the maximum fEPSP amplitude followed by 20min recordings (200ms pulses delivered every 20s) to obtain a stable fEPSP baseline. Stimulus-response curves were obtained from fEPSPs slopes and synaptic potentiation was induced by weak theta burst stimulation (wTBS; two bursts of four pulses at 100 Hz spaced by 200 ms). The following drugs were bath applied to brain slices: tetrodotoxin (1μM), methyllycaconitine citrate (MLA, Tocris, 10nM), 6-cyano-7-nitroquinoxaline-2,3-dione (CNQX, Sigma, 10uM), d-(−)-2-Amino-5-phosphonopentanoic acid (dAP5, Sigma, 30μM), picrotoxin (PTX, Sigma, 10uM), mecamylamine hydrochloride (MEC, Sigma, 25μM), and (−)-Nicotine ditartrate (Nic, Tocris, 1μM).

Voltage Imaging

We loaded the dye RH795 (Invitrogen) extracellularly by diluting the dye to 1mg/ml in ACSF and incubating hippocampal slices for 5 min constantly bubbled with 95% O_2 and 5% CO_2. The red shifted dye DI-4-ANBDQPQ[23] was diluted in absolute ethanol and ejected over the slice under a rapid flow of ACSF. PC voltage sensitive dye (VSD) loading (di-1-ANEPPQ)[50] via patch pipettes was performed as described previously[21] but with the internal solution supplemented with the Na^+ channel blocker QX314. For VSD electroporation, a solution containing 5mg/ml of di-1-ANEPPQ in the recording internal solution was loaded into glass pipettes and injected into PCs from a distance of 5–10 μm by applying 1–3 +10mV/500μs pulses on the vicinity of cell somas. After electroporation, we allowed the tissue to rest for 1.5–2h before recordings to assure VSD spread into the dendrite. Image series, acquired by a sCMOS camera or a EM-CCD (Neo, Andor, Ireland) were produced by exciting the sample with a 200W metal-halide lamp through a bandpass filter centered at 535nm (~510 to 560nm pass) and collecting the emission through a longpass filter (590nm-cutt off) or using a LED array (627nm, Luxeon) excitation source through a ET640/30x filter (Chrona), a Q680LP splitter and a HQ705LP emission filter (Chroma). Image acquisition and extracellular stimulation was synchronized through TTL pulses. To guarantee time precision, the stimulator and the camera 'fire' outputs (that flags image acquisition) were recorded using a National Instruments DAQ card and a custom imaging/electrophysiology software ('KiaFluo'[51]). All electrophysiology and voltage imaging experiments were performed at 30°C.

Single-cell reverse transcriptase PCR

External and internal solutions used for experiments in which cells were collected for single-cell PCR were filtered with a 0.2 μm pore diameter filter. After recordings, the cytoplasm and organelles were sucked into the recording pipette tip as previously described[52]. Pipettes were quickly removed and tips were broken into 1.5 mL tubes containing freshly prepared solution of 20U of RNase inhibitor and 8.3mM DTT; samples were frozen immediately on dry ice and stored at −80°C until use. The samples were thawed on ice and the RNA converted to cDNA by reverse transcription for 1hr using 0.5mM dNTPs mix, 1.25μM random primers, 40U of RNase inhibitor, 100U of M-MLV RT (Invitrogen), 50mM Tris-HCl, 75mM KCl and 3mM MgCl2, pH 8.3. The RT enzyme was denatured and the cDNAs stored at −80°C until use. A first round of PCR was performed using 1.5mM MgCl2, 10pmol of each primer, 1.0U of platinum Taq-DNA polymerase (Invitrogen), 20mM Tris-HCl and 50mM KCl pH 8.4. Thermal cycles consisted of an initial denaturation step of 94°C

NIH-PA Author Manuscript

NIH-PA Author Manuscript

NIH-PA Author Manuscript

for 2 min, followed by 35 cycles of 94°C for 50s, 55°C for 45s and 72°C for 45s. A second nested PCR was then performed as mentioned above using 10% of the first PCR reaction as template. All PCR products were resolved on 2.5% agarose gels. Primers were designed based upon sequences deposited in the GenBank database (www.ncbi.nlm.nih.gov/nucleotide). The *Gad67* primers used were GAD67nl-up CCAATAGCCTGGAAGAGAAGAG; GAD67nl-lw TCCCATCACCATCTTTATTTGA to generate the first round product and GAD67s-up GTCCTCCAAGAACCTGCTTTC; GAD67s-lw TCAGCCATTCACCAGCTAAAC to generate the second round product.

In situ hybridization

Construction of *in situ* probes is described elsewhere[53]. The *Viaat* clone is commercially available at Invitrogen (Clone ID: 5717808) and corresponds to nucleotides 2021–2805 (NM_009508). The mouse Somatostatin full length cDNA clone IRAVp968G0228D was obtained from Source BioSciences. Antisense and sense transcripts were generated by in-vitro transcription using either T7 or SP6 polymerase and labeled with digoxygenin (Roche) following manufacturer's instructions to make in-situ hybridization (ISH) probes. Both sense and antisense probes were tested on adjacent brain sections and specificity of the antisense ISH probe was verified (not shown). The floating *in situ* hybridization was done as previously described[54], with the exclusion of the graded methanol series and with the hybridization temperature set to 58°C. Signal detection was made by Fast Red tablets (Roche Diagnostics Scandinavia). After development, the tissue was washed in phosphate buffered saline with Tween-20 (0,1 %, MP biomedicals) and mounted on glass slides. Sections were subsequently stained with antibody against Red Fluorescent Protein (RFP; Abcam; catalogue no: ab62341; Rabbit; 1:200) to re-visualize the Tomato+ neurons that were bleached by the *in situ* hybridization protocol. Next, slices were incubated 3 hrs at room temperature in secondary antibody (donkey anti-rabbit; Invitrogen; Alexa 488; 1:400). Images were collected on a Zeiss LSM 510 Meta confocal microscope and stacked using Volocity software (Improvision) and edited in Photoshop CS3 (Adobe), where the color palette was adjusted for consistency (RFP - *red* and Viaat, Somatostatin – *green*).

Virus injection

Chrna2-cre and Chrna2-cre/*Viaat*^{lx} mice (1–2 months old), sometimes crossed with *R26*^{tom} reporter mice, were anaesthetized with a cocktail of one part of Hypnorm (fentanyl citrate 0.315 mg/ml, fluanisone 10 mg/ml; VetaPharma), one part of midazolam (5 mg/ml) in two parts of distilled water (subcutaneous injection of 0.075 ml/10g of weight). Animals were placed in a stereotaxic frame (Stoelting) and viral particles (1.6×10^{13} particles/ml of AAV2/9.EF1a.DIO.hChR2(H134R)-EYFP.WPRE.hGH (Addgene vector 20298), obtained from the University of Pennsylvania Vector Core Facility) were injected unilaterally into the dorsal hippocampus (CA1) using the following bregma coordinates: −3.2 mm AP, +3.8 mm ML, and 3.6/2.6 mm DV. Virus solution (0.75µl/injection depth) was delivered at a flow rate of 200 nl/min using an electronic pump (World Precision Instruments) equipped with a 10µl Hamilton syringe. After infusion, the needle was left in place for one minute. The scalp incision was sutured and animals were housed in special containment cages after recovering from anesthesia. *In vitro* recordings were performed within 10–14 days of virus injection.

Statistical Analysis

Statistical analysis of electrophysiology data was performed by two-tailed paired or unpaired *t*-tests (homogeneity of variances was tested using Levene's test). Data are presented as mean ± s.e.m. (standard error of the mean); $p \leq 0.05$ was considered as statistically significant.

NIH-PA Author Manuscript

NIH-PA Author Manuscript

NIH-PA Author Manuscript

Supplementary Material

Refer to Web version on PubMed Central for supplementary material.

Acknowledgments

We thank G. Buzsaki, P. Ascher, B. Lamotte d'Incamps, O. Amaral and E. Hanse for comments on earlier versions of this manuscript. Supported by the foundations of Märta och Kjell Beijer, Hållsten, Göran Gustafsson, The Swedish Foundation for International Cooperation in Research and Higher Education (STINT), Brazilian Federal Agency for Support and Evaluation of Graduate Education (CAPES), Brazilian National Council of Technological and Scientific Development (CNPq), Research Support Agency of the State of Rio Grande do Norte (FAPERN), NIH grant R01EB001963, Swedish Medical Research Council, Swedish Brain Foundation and Uppsala University. KK is a Royal Swedish Academy of Sciences Research Fellow supported by a grant from the Knut and Alice Wallenberg Foundation.

References

1. Morris RG, Garrud P, Rawlins JN, O'Keefe J. Place navigation impaired in rats with hippocampal lesions. Nature. 1982; 297:681–683. [PubMed: 7088155]
2. Eichenbaum H. Hippocampus: cognitive processes and neural representations that underlie declarative memory. Neuron. 2004; 44:109–120. [PubMed: 15450164]
3. Murray AJ, et al. Parvalbumin-positive CA1 interneurons are required for spatial working but not for reference memory. Nat Neurosci. 2011; 14:297–299. [PubMed: 21278730]
4. Korotkova T, Fuchs EC, Ponomarenko A, von Engelhardt J, Monyer H. NMDA receptor ablation on parvalbumin-positive interneurons impairs hippocampal synchrony, spatial representations, and working memory. Neuron. 2010; 68:557–569. [PubMed: 21040854]
5. Freund TF, Buzsaki G. Interneurons of the hippocampus. Hippocampus. 1996; 6:347–470. [PubMed: 8915675]
6. Somogyi P, Klausberger T. Defined types of cortical interneurone structure space and spike timing in the hippocampus. J Physiol. 2005; 562:9–26. [PubMed: 15539390]
7. Ascoli GA, et al. Petilla terminology: nomenclature of features of GABAergic interneurons of the cerebral cortex. Nat Rev Neurosci. 2008; 9:557–568. [PubMed: 18568015]
8. Gradinaru V, et al. Molecular and cellular approaches for diversifying and extending optogenetics. Cell. 2010; 141:154–165. [PubMed: 20303157]
9. Maccaferri G, McBain CJ. Passive propagation of LTD to stratum oriensalveus inhibitory neurons modulates the temporoammonic input to the hippocampal CA1 region. Neuron. 1995; 15:137–145. [PubMed: 7619518]
10. Tort AB, Rotstein HG, Dugladze T, Gloveli T, Kopell NJ. On the formation of gamma-coherent cell assemblies by oriens lacunosum-moleculare interneurons in the hippocampus. Proc Natl Acad Sci U S A. 2007; 104:13490–13495. [PubMed: 17679692]
11. Gloveli T, et al. Orthogonal arrangement of rhythm-generating microcircuits in the hippocampus. Proc Natl Acad Sci U S A. 2005; 102:13295–13300. [PubMed: 16141320]
12. Rotstein HG, et al. Slow and fast inhibition and an H-current interact to create a theta rhythm in a model of CA1 interneuron network. J Neurophysiol. 2005; 94:1509–1518. [PubMed: 15857967]
13. Wulff P, et al. Hippocampal theta rhythm and its coupling with gamma oscillations require fast inhibition onto parvalbumin-positive interneurons. Proc Natl Acad Sci U S A. 2009; 106:3561–3566. [PubMed: 19204281]
14. Nakauchi S, Brennan RJ, Boulter J, Sumikawa K. Nicotine gates longterm potentiation in the hippocampal CA1 region via the activation of alpha2* nicotinic ACh receptors. Eur J Neurosci. 2007; 25:2666–2681. [PubMed: 17466021]
15. Cutsuridis V, Cobb S, Graham BP. Encoding and retrieval in a model of the hippocampal CA1 microcircuit. Hippocampus. 2010; 20:423–446. [PubMed: 19489002]
16. Hasselmo ME. Neuromodulation: acetylcholine and memory consolidation. Trends Cogn Sci. 1999; 3:351–359. [PubMed: 10461198]

NIH-PA Author Manuscript NIH-PA Author Manuscript NIH-PA Author Manuscript

17. Ishii K, Wong JK, Sumikawa K. Comparison of alpha2 nicotinic acetylcholine receptor subunit mRNA expression in the central nervous system of rats and mice. J Comp Neurol. 2005; 493:241–260. [PubMed: 16255031]
18. Jia Y, Yamazaki Y, Nakauchi S, Sumikawa K. Alpha2 nicotine receptors function as a molecular switch to continuously excite a subset of interneurons in rat hippocampal circuits. Eur J Neurosci. 2009; 29:1588–1603. [PubMed: 19385992]
19. Jia Y, Yamazaki Y, Nakauchi S, Ito K, Sumikawa K. Nicotine facilitates long-term potentiation induction in oriens-lacunosum moleculare cells via Ca2+ entry through non-alpha7 nicotinic acetylcholine receptors. Eur J Neurosci. 2010; 31:463–476. [PubMed: 20113344]
20. Maccaferri G, McBain CJ. The hyperpolarization-activated current (Ih) and its contribution to pacemaker activity in rat CA1 hippocampal stratum oriensalveus interneurones. J Physiol. 1996; 497(Pt 1):119–130. [PubMed: 8951716]
21. Palmer LM, Stuart GJ. Site of action potential initiation in layer 5 pyramidal neurons. J Neurosci. 2006; 26:1854–1863. [PubMed: 16467534]
22. Tong Q, Ye C-P, Jones JE, Elmquist JK, Lowell BB. Synaptic release of GABA by AgRP neurons is required for normal regulation of energy balance. Nat Neurosci. 2008; 11:998–1000. [PubMed: 19160495]
23. Kee MZ, Wuskell JP, Loew LM, Augustine GJ, Sekino Y. Imaging activity of neuronal populations with new long-wavelength voltage-sensitive dyes. Brain Cell Biol. 2008; 36:157–172. [PubMed: 19219551]
24. Cardin JA, et al. Targeted optogenetic stimulation and recording of neurons in vivo using cell-type-specific expression of Channelrhodopsin-2. Nat Protoc. 2010; 5:247–254. [PubMed: 20134425]
25. Maccaferri G, Dingledine R. Control of feedforward dendritic inhibition by NMDA receptor-dependent spike timing in hippocampal interneurons. J Neurosci. 2002; 22:5462–5472. [PubMed: 12097498]
26. Pouille F, Scanziani M. Enforcement of temporal fidelity in pyramidal cells by somatic feed-forward inhibition. Science. 2001; 293:1159–1163. [PubMed: 11498596]
27. Maccaferri G, Roberts JD, Szucs P, Cottingham CA, Somogyi P. Cell surface domain specific postsynaptic currents evoked by identified GABAergic neurones in rat hippocampus in vitro. J Physiol. 2000; 524(Pt 1):91–116. [PubMed: 10747186]
28. Tu B, Gu Z, Shen JX, Lamb PW, Yakel JL. Characterization of a nicotine-sensitive neuronal population in rat entorhinal cortex. J Neurosci. 2009; 29:10436–10448. [PubMed: 19692619]
29. Blasco-Ibanez JM, Freund TF. Synaptic input of horizontal interneurons in stratum oriens of the hippocampal CA1 subfield: structural basis of feed-back activation. Eur J Neurosci. 1995; 7:2170–2180. [PubMed: 8542073]
30. Minneci F, et al. Signaling properties of stratum oriens interneurons in the hippocampus of transgenic mice expressing EGFP in a subset of somatostatincontaining cells. Hippocampus. 2007; 17:538–553. [PubMed: 17455332]
31. Veruki ML, Oltedal L, Hartveit E. Electrical coupling and passive membrane properties of AII amacrine cells. J Neurophysiol. 2010; 103:1456–1466. [PubMed: 20089813]
32. Gulyas AI, Gorcs TJ, Freund TF. Innervation of different peptidecontaining neurons in the hippocampus by GABAergic septal afferents. Neuroscience. 1990; 37:31–44. [PubMed: 1978740]
33. Gulyas AI, et al. Parvalbumin-containing fast-spiking basket cells generate the field potential oscillations induced by cholinergic receptor activation in the hippocampus. J Neurosci. 2010; 30:15134–15145. [PubMed: 21068319]
34. Klausberger T, et al. Spike timing of dendrite-targeting bistratified cells during hippocampal network oscillations in vivo. Nat Neurosci. 2004; 7:41–47. [PubMed: 14634650]
35. Taniguchi H, et al. A resource of Cre driver lines for genetic targeting of GABAergic neurons in cerebral cortex. Neuron. 2011; 71:995–1013. [PubMed: 21943598]
36. Fuchs EC, et al. Recruitment of parvalbumin-positive interneurons determines hippocampal function and associated behavior. Neuron. 2007; 53:591–604. [PubMed: 17296559]
37. Cardin JA, et al. Driving fast-spiking cells induces gamma rhythm and controls sensory responses. Nature. 2009; 459:663–667. [PubMed: 19396156]

NIH-PA Author Manuscript

NIH-PA Author Manuscript

NIH-PA Author Manuscript

38. Lovett-Barron M, et al. Regulation of neuronal input transformations by tunable dendritic inhibition. Nat Neurosci. 2012; 15:423–30. [PubMed: 22246433]
39. Elfant D, Pál BZ, Emptage N, Capogna M. Specific inhibitory synapses shift the balance from feedforward to feedback inhibition of hippocampal CA1 pyramidal cells. Eur J Neurosci. 2008; 27:104–13. [PubMed: 18184315]
40. Kim S, Guzman SJ, Hu H, Jonas P. Active dendrites support efficient initiation of dendritic spikes in hippocampal CA3 pyramidal neurons. Nat Neurosci. 2012; 15:600–6. [PubMed: 22388958]
41. Colom LV. Septal networks: relevance to theta rhythm, epilepsy and Alzheimer's disease. J Neurochem. 2006; 96:609–623. [PubMed: 16405497]
42. Davis JA, Gould TJ. Associative learning, the hippocampus, and nicotine addiction. Curr Drug Abuse Rev. 2008; 1:9–19. [PubMed: 19630701]
43. Lynch MA. Long-term potentiation and memory. Physiol Rev. 2004; 84:87–136. [PubMed: 14715912]
44. Dugladze T, et al. Impaired hippocampal rhythmogenesis in a mouse model of mesial temporal lobe epilepsy. Proc Natl Acad Sci U S A. 2007; 104:17530–17535. [PubMed: 17954918]
45. Neymotin SA, et al. Ketamine disrupts theta modulation of gamma in a computer model of hippocampus. J Neurosci. 2011; 31:11733–11743. [PubMed: 21832203]
46. Stanley EM, Fadel JR, Mott DD. Interneuron loss reduces dendritic inhibition and GABA release in hippocampus of aged rats. Neurobiol Aging. 2012; 33:431 e1–13. [PubMed: 21277654]
47. Fraklin, KBJ.; Paxinos, G. The Mouse Brain in Stereotaxic Coordinates. 3rd Edition. Elsevier; 2007.
48. Marshall VM, Allison J, Templeton T, Foote SJ. Generation of BAC transgenic mice. Methods Mol Biol. 2004; 256:159–182. [PubMed: 15024166]
49. Leao RN, Tan HM, Fisahn A. Kv7/KCNQ channels control action potential phasing of pyramidal neurons during hippocampal gamma oscillations in vitro. J Neurosci. 2009; 29:13353–13364. [PubMed: 19846723]
50. Zhou WL, Yan P, Wuskell JP, Loew LM, Antic SD. Intracellular long-wavelength voltage-sensitive dyes for studying the dynamics of action potentials in axons and thin dendrites. J Neurosci Methods. 2007; 164:225–239. [PubMed: 17560661]
51. Leao RN, et al. A voltage-sensitive dye-based assay for the identification of differentiated neurons derived from embryonic neural stem cell cultures. PloS One. 2010; 5:e13833. [PubMed: 21079795]
52. Leao RN, Colom LV, Borgius L, Kiehn O, Fisahn A. Medial septal dysfunction by Abeta-induced KCNQ channel-block in glutamatergic neurons. Neurobiol Aging. 2011
53. Gezelius H, Wallen-Mackenzie A, Enjin A, Lagerstrom M, Kullander K. Role of glutamate in locomotor rhythm generating neuronal circuitry. J Physiol Paris. 2006; 100:297–303. [PubMed: 17618093]
54. Enjin A, et al. Identification of novel spinal cholinergic genetic subtypes disclose Chodl and Pitx2 as markers for fast motor neurons and partition cells. J Comp Neurol. 2010; 518:2284–2304. [PubMed: 20437528]

NIH-PA Author Manuscript

NIH-PA Author Manuscript

NIH-PA Author Manuscript

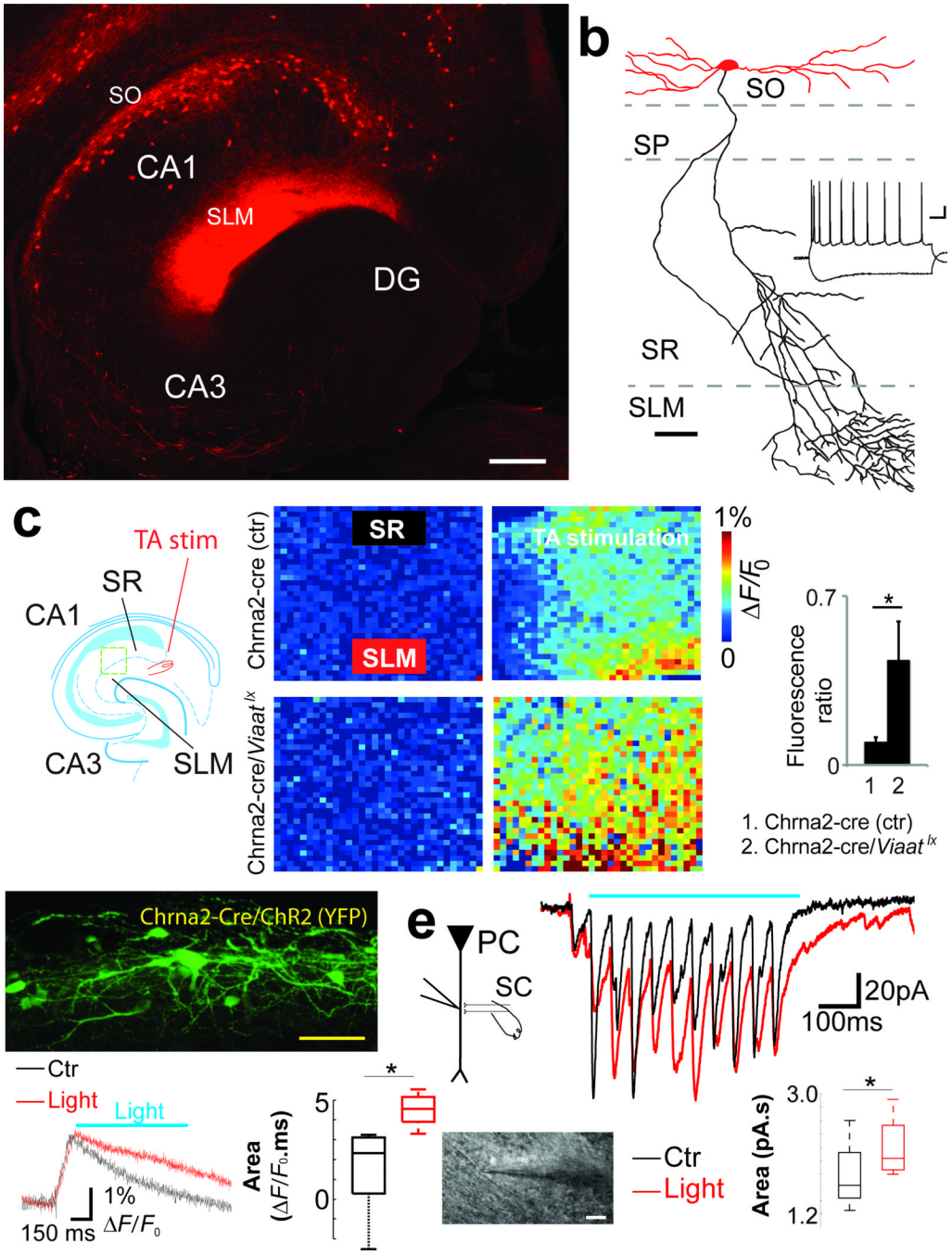

Figure 1. *Chrna2* is a marker for CA1 OLM interneurons

(**a**) Photomicrograph of a horizontal hippocampal slice of a Chrna2-Cre/*R26*^{tom} mouse showing the distribution of Tomato+ cell bodies in SO. Note dense axonal arborizations of Tomato+ cells in SLM and the absence of Tomato+ cell bodies in CA3 or DG (scale bar=100μm). (**b**) Reconstruction of a biocytin filled Tomato+ neuron (scale bar=20μm, dendrites-red, axon-black); *right inset*, typical membrane response of a hippocampal Tomato + neuron to hyper- and depolarizing current injection (scale bar=100ms/15mV). (**c**) Diagram of experimental setup (left) with TA stimulation (red) and green box delineating where VSD imaging was performed. The hippocampus diagram was adapted from ref. 47. VSD

NIH-PA Author Manuscript

NIH-PA Author Manuscript

NIH-PA Author Manuscript

fluorescent responses to TA stimulation (10 pulses, 20Hz) were measured at rectangular regions in SR (black) and SLM (red). The excitation spread was defined as the ratio between the fluorescence variation in SR and SLM, measured 50ms after stimulus onset. Results comparing Chrna2-cre and Chrna2-cre/*Viaat*^{lx} mice are shown in the right bar graph. Error bars denote ± s.e.m. (**d**) Expression of ChR2/YFP in Chrna2-cre cells in a hippocampal slice used for VSD imaging + optogenetic stimulation of OLM^{ChR2} cells (top). Fluorescence changes at SR following SC stimulation in control with or without application of a 1.4mW laser light pulse (bottom left). Excitation of OLM^{ChR2} cells with light produced an increase in the depolarization at SR following SC stimulation measured as the area under the curve of the fluorescence signal change in response to SC stimulation (bottom right). (**e**) Schematic and image of a PC dendritic voltage clamp recording at SR (left). Recordings of typical traces show excitation from AMPA EPSCs (isolated by blocking NMDA with dAP5) elicited by SC stimulation in control (black) and during blue light stimulation (horizontal bar) targeted at CA1 SO (red). The boxplot shows increased summation of AMPA mediated EPSCs during blue light stimulation of the CA1 SO region (red) compared to no light stimulation (black). *p<0.05.

NIH-PA Author Manuscript
NIH-PA Author Manuscript
NIH-PA Author Manuscript

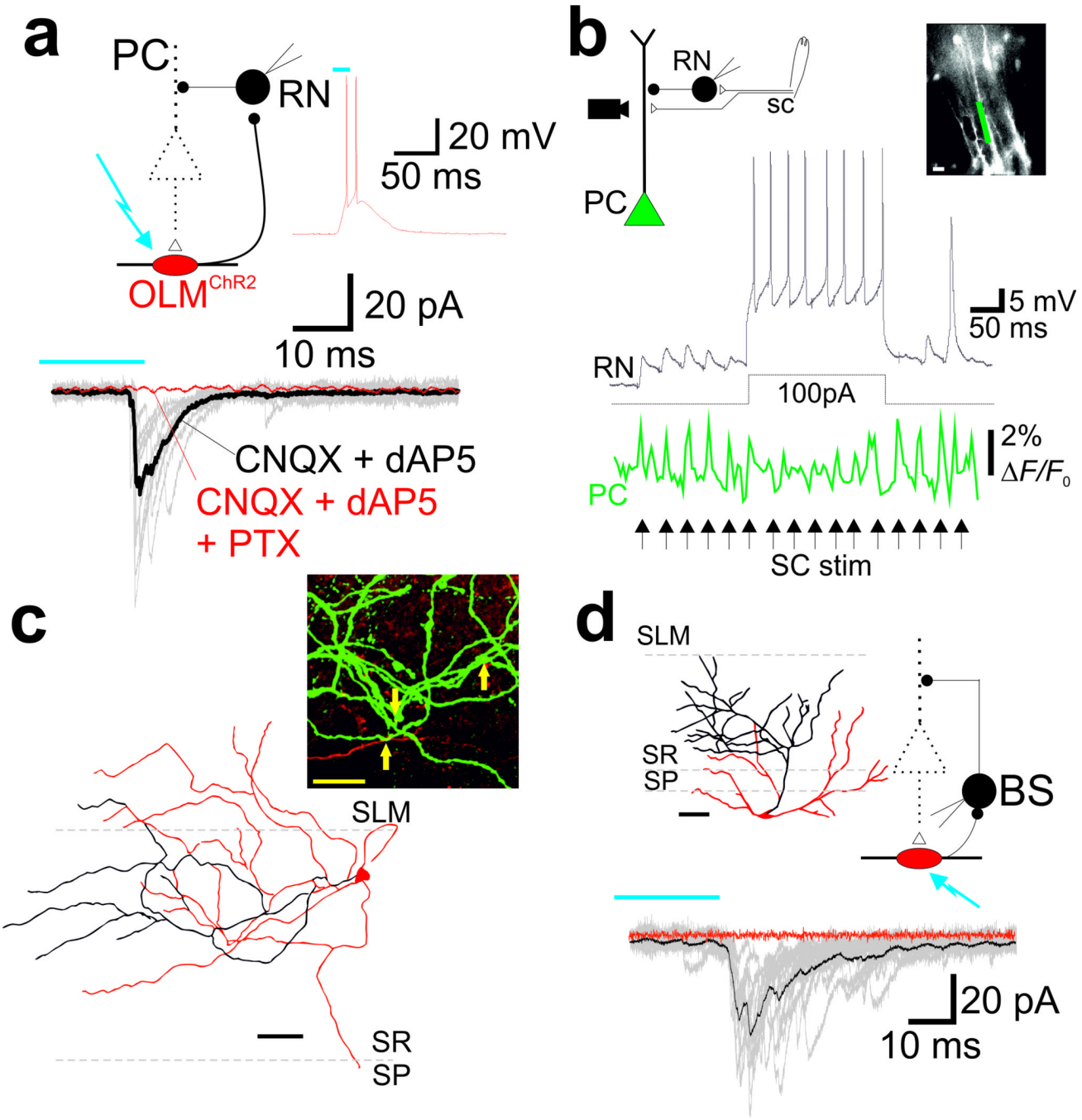

Figure 2. OLM$^{\alpha 2}$ cells inhibit interneurons that synapse on PC proximal dendrites

(**a**) Schematic of experimental setup (upper left). IPSCs in an SR interneuron (RN) were elicited by 20ms light pulse stimulation of OLM$^{\alpha 2}$ cells transduced with Cre-inducible hChR2 (OLM^{ChR2}). Glutamatergic EPSCs were blocked by dAP5 and CNQX. Application of picrotoxin (PTX) abolished the postsynaptic response to blue light. *Inset*, APs triggered in an OLM^{ChR2} cell by a 20ms light pulse. (**b**) Current clamp recordings showing EPSPs in the same SR interneuron as in **a** (black) elicited by SC stimulation (arrows). RN spiking elicited by concomitant current injection during SC stimulation lowered post-synaptic PC responses, as evidenced by voltage imaging of PCs electroporated with VSD. Changes in potential

NIH-PA Author Manuscript

NIH-PA Author Manuscript

NIH-PA Author Manuscript

were measured at the region of interest delimited by the green rectangle shown on the top right micrograph; scale bar=20μm. (**c**) Bottom, reconstruction of the SR interneuron (filled with biocytin) shown in **a** and **b**. Top, confocal imaging showing synaptic contacts (arrows) between OLM cell axons (red) and RN dendrites (green). Scale bar=20μm. (**d**) IPSCs in a bistratified interneuron (BS) elicited by 20ms light pulse stimulation of OLM^{ChR2} cells. The reconstruction of the BS interneuron is shown on the top left panel. Scale bar=50μm.

NIH-PA Author Manuscript

NIH-PA Author Manuscript

NIH-PA Author Manuscript

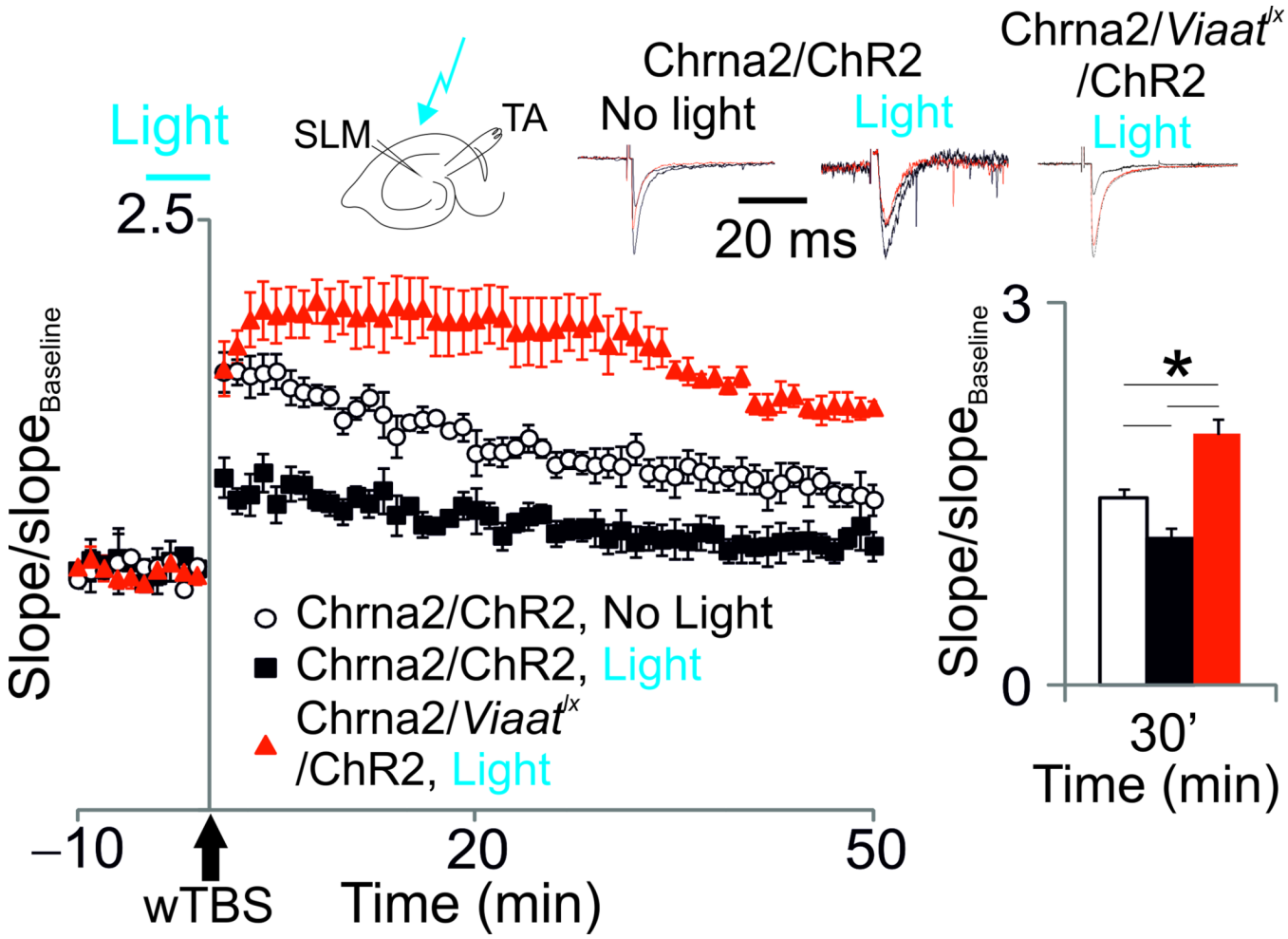

Figure 3. OLM$^{\alpha 2}$ cells suppress LTP in the TA pathway

Potentiation of TA synapses after wTBS in hippocampal slices of animals transduced with hChR2 (Chrna2-cre/ChR2 and Chrna2-cre/*Viaat*^{lx}/ChR2 mice) in control conditions (no light) and when a light pulse was applied 5 min prior to and during TA wTBS (see **Methods**). Top traces show fEPSPs before (black line), 10 min (dashed black line) and 30 min (red line) after wTBS (normalized to the peak amplitude). Bar graphs show the mean normalized slope 30 min after wTBS (*p<0.05). Error bars denote ± s.e.m. Schematic shows overview of stimulation setup.

NIH-PA Author Manuscript

NIH-PA Author Manuscript

NIH-PA Author Manuscript

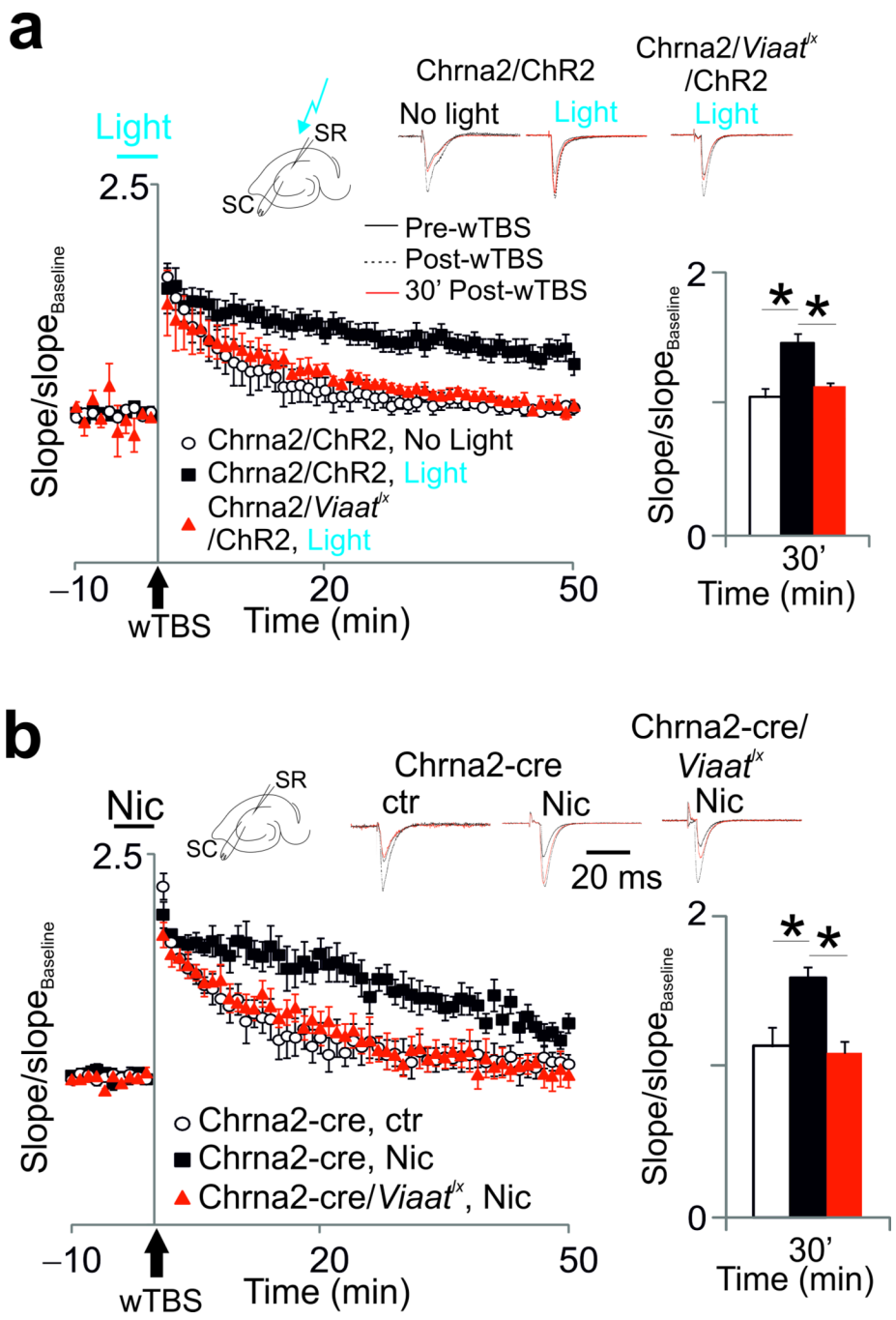

Figure 4. OLM$^{\alpha 2}$ cells enhance LTP in the SC pathway

(**a**) Potentiation of SC synapses in Chrna2-cre/ChR2 and Chrna2-cre/*Viaat*^{Ix}/ChR2 mice in control conditions (no light) and with a light pulse applied 5 min prior to and during SC wTBS. Top traces show normalized fEPSPs before (black line), 10 min (dashed black line) and 30 min (red line) after wTBS. Bar graphs show the mean normalized slope 30 min after wTBS. Error bars denote ± s.e.m. (**b**) Same as in **a**, but with 1μM bath-applied nicotine instead of light stimulation. Schematics show overview of stimulation setups.

NIH-PA Author Manuscript
NIH-PA Author Manuscript
NIH-PA Author Manuscript

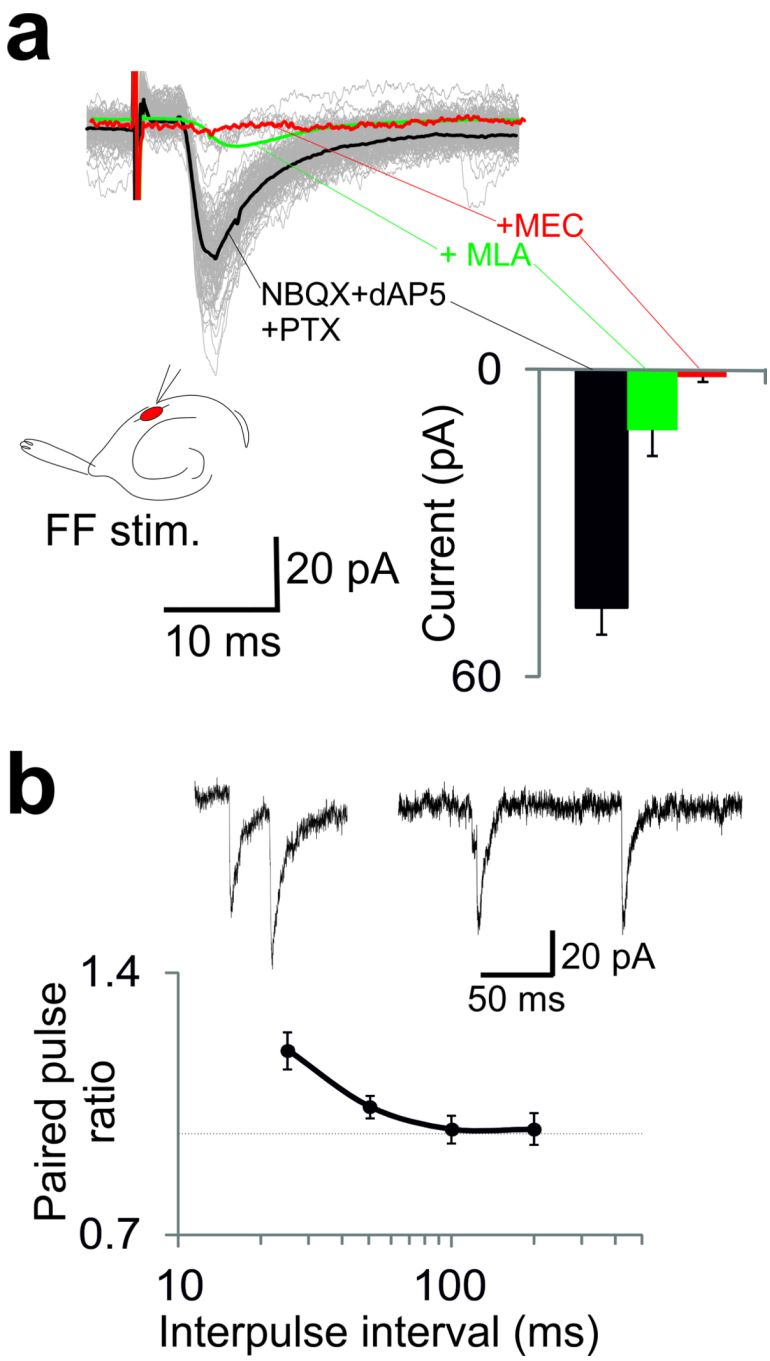

Figure 5. OLM$^{\alpha 2}$ cells receive remote cholinergic input

(**a**) Cholinergic EPSCs elicited by FF stimulation (gray; isolated by the application of glutamate and GABA receptor blockers; the black trace shows the average EPSC). The average EPSCs after the addition of the α7-blocker MLA (green trace) and the nicotine blocker MEC (red trace) are also shown. Peak EPSC amplitudes are shown on the right bar graph. Error bars denote ± s.e.m. Schematic shows overview of stimulation setup. (**b**) Average paired pulse ratio of FF-induced cholinergic EPSC in OLM$^{\alpha 2}$ cells as a function of the inter-pulse interval. Error bars denote ± s.e.m. The top traces show examples of 25ms (left) and 100ms (right) inter-pulse intervals.